Journal of Alloys and Compounds 509 (2011) 5341–5348

Contents lists available at ScienceDirect

Journal of Alloys and Compounds

journal homepage: www.elsevier.com/locate/jallcom

Fabrication and characterization of dendrimer-encapsulated monometallic Co nanoparticles

H. Kavas [a], Z. Durmus [b], E. Tanrıverdi [b], M. Şenel [b], H. Sozeri [c], A. Baykal [b,*]

[a] Department of Physics, Fatih University, B. Cekmece, 34500 Istanbul, Turkey
[b] Department of Chemistry, Fatih University, B. Cekmece, 34500 Istanbul, Turkey
[c] TUBITAK-UME, National Metrology Institute, PO Box 54, 41470 Gebze-Kocaeli, Turkey

ARTICLE INFO

Article history:
Received 8 January 2011
Received in revised form 4 February 2011
Accepted 7 February 2011
Available online 24 February 2011

Keywords:
Dendrimer
Cobalt
XPS
Chemical synthesis
Magnetic properties

ABSTRACT

A series of cobalt (Co) nanoparticles were synthesized by employing PAMAM dendrimers with different generations (G 0.0–3.0) as templates and sodium borohydride as a reducing agent. Extensive characterizations of the products were done using TEM, FT-IR, VSM, TGA, and XPS. The magnetization curves have superparamagnetic non hysteric characteristic at lower fields and with nonsaturation characteristic at high fields. All XRD patterns indicate that amorphous structure of all products. The shake-up satellites are observed at higher energies of the XPS peaks.

1. Introduction

Magnetic nanoparticles (MP) exhibit enhanced magnetic, optical, and electrical properties when compared with their bulk counterparts rendering nanoparticles of interest for a variety of applications information storage [1,2], color imaging [3], magnetic refrigeration [4], ferro-fluids [5], cell sorting [6], medical diagnosis [7], and controlled drug delivery [8]. Most of these applications require chemically stable, well-dispersed and uniform size particles. For this reason, new technologies in synthesis and methods of analysis have been developed.

Dendrimers are very exiting cascade type three-dimensional polymers that have well-defined molecular weight/size, uniform dense terminal functional groups, and porosity. Generally, dendrimers of low generation tend to exist in relatively open forms, at higher generations ($G \geq 4.0$) take intrinsically well-defined globular structure. Dendrimers might provide reaction sites including their interior or periphery. Accordingly, it is expected that the use of dendrimers as templates/stabilizers for the synthesis of nanoparticles are affected by the generation of dendrimers and show different behavior from those prepared using conventional linear polymers [9]. A poly-amidoamine (PAMAM) dendrimer is highly branched macromolecule that contains interior tertiary amine groups which can effectively make coordination with metal ions. Such metal ions may then be reduced to form encapsulated metal particles that can be highly stable in solution. Since the same number of chelating sites is present in all dendrimer molecules, this process can yield mono-disperse metal particles [10–12].

Dendrimer-stabilized nanoparticles (DSN) may provide one avenue toward controlled synthesis of supported metal catalysts. Dendrimers are a special class of hyper branched polymers with a specific molecular structure and controllable size. At higher generation, they possess a very dense exterior, while containing hollow pockets that can be ideal for use as nano-scale containers [12]. This property finds widespread application in catalysis and biomedical research. Dendrimers containing metal nanoparticles also find applications in catalysis [13,14]. It is possible to produce dendrimer–metal nanocomposites by the following routes: (1) forming of complexes by binding of metal ions to a template of dendrimer molecules and (2) nanoclusture forming by immobilization of the metal ions onto dendrimer templates. Composition, size and structure of the system also strongly affect the properties of dendrimer–metal nanocomposites [15–18].

In this study, the synthesis of Co nanoparticles via the template of PAMAM dendrimers with different generation was presented. Extensive characterizations of the fabricated nanocomposites have been performed by using a variety of microscopy and spectroscopic techniques.

* Corresponding author. Tel.: +90 212 866 33 00/2061; fax: +90 212 866 34 02.
E-mail address: hbaykal@fatih.edu.tr (A. Baykal).

0925-8388/$ – see front matter © 2011 Elsevier B.V. All rights reserved.
doi:10.1016/j.jallcom.2011.02.038

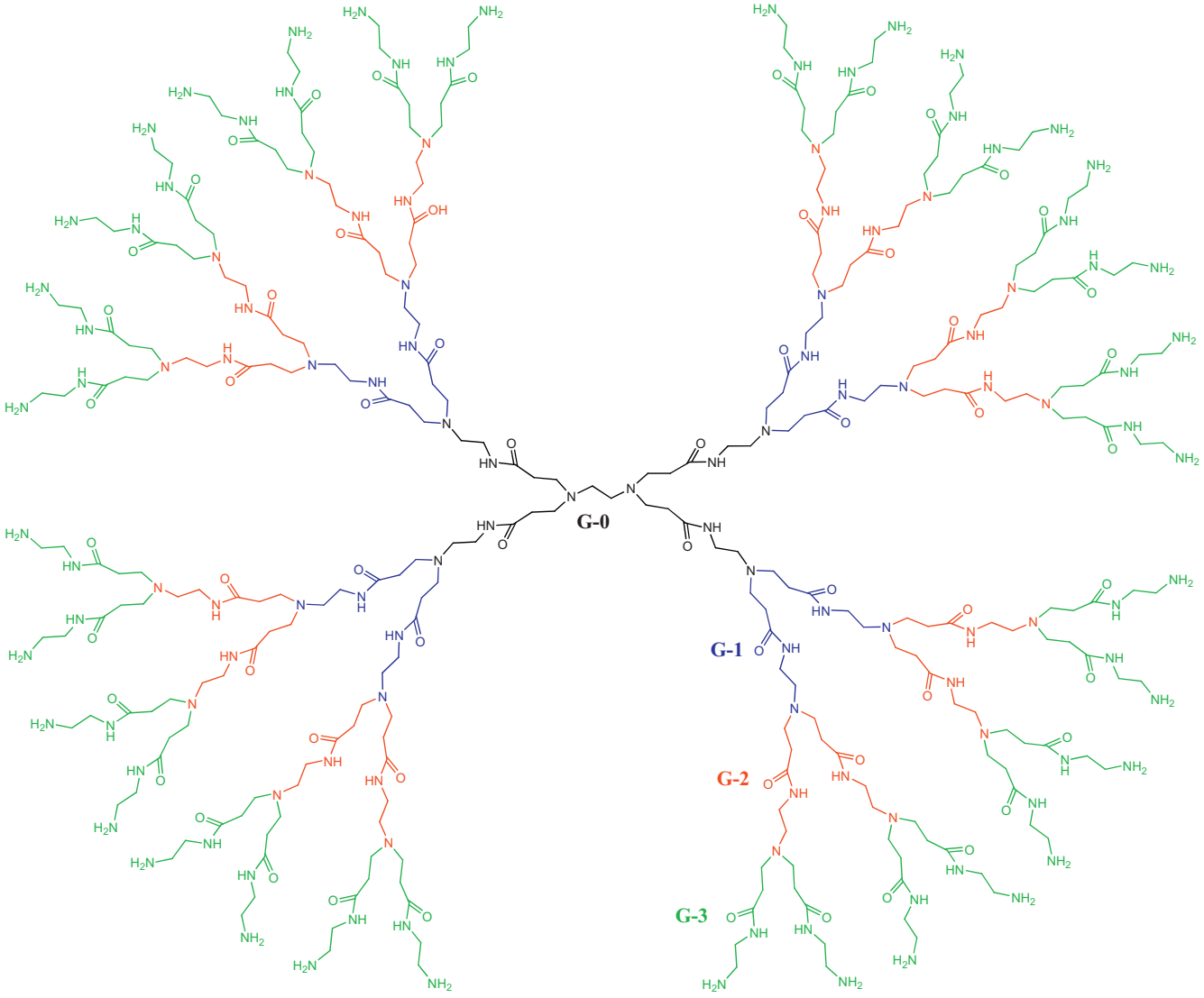

Fig. 1. The structure of G0.0–G3.0 dendrimers.

2. Experimental

2.1. Materials

Cobalt chloride ($CoCl_2 \cdot 6H_2O$), sodium borohydride ($NaBH_4$), were purchased from Merck and used as received without further purification. All the chemicals are of analytical grade.

2.2. Characterization

X-ray powder diffraction (XRD) analysis was conducted on a Rigaku Smart Lab Diffractometer operated at 40 kV and 35 mA using Cu Kα radiation (λ = 1.54178 Å).

Fourier transform infrared (FT-IR) spectra were recorded in transmission mode with a Perkin Elmer BX FT-IR infrared spectrometer. The powder samples were ground with KBr and compressed into a pellet (in the range 4000–400 cm^{-1}).

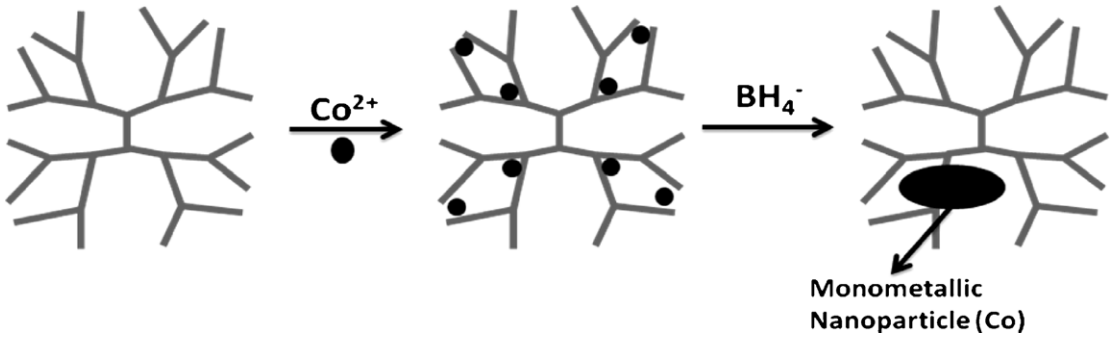

Fig. 2. Schematic representation of the synthesis of dendrimer encapsulated Co nanoparticles.

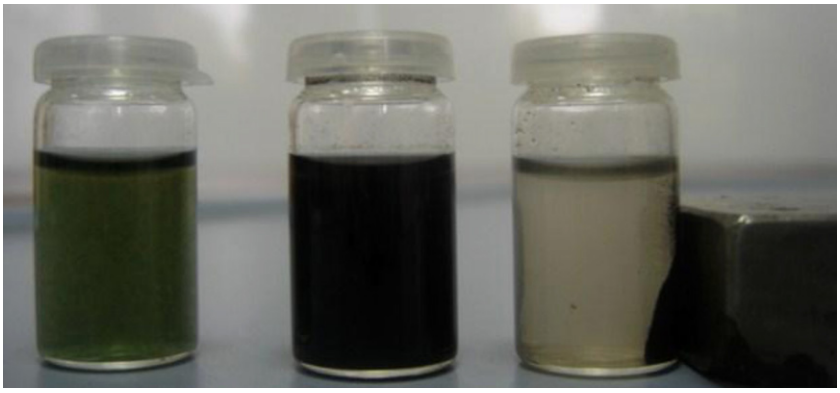

Fig. 3. Changes in solution color of G220–Co^{2+} before (a) and after reduction (b) and the collection of Co nanoparticles by a magnet (c).

Transmission electron microscopy (TEM) analysis was performed using a JEOL JEM 2100 microscope. A drop of diluted sample in alcohol was dripped on a TEM grid.

The thermal stability was determined by thermogravimetric analysis (TGA, Perkin Elmer Instruments model, STA 6000). The TGA thermograms were recorded for 5 mg of powder sample at a heating rate of 10 °C min in the temperature range of 30–800 °C under nitrogen atmosphere.

VSM measurements were performed by using a Quantum Design Vibrating sample magnetometer (QD-VSM). The sample was measured between ±10 kOe at room temperature and 10 K. ZFC (zero field cooling) and FC (field cooling) measurements were carried out at 100 Oe and the blocking temperature was determined from the measurements.

XPS analysis using Phobus 150 Specs electron analyzer with conventional X-ray source (AlKa).

2.3. Synthesis

2.3.1. The synthesis of dendrimers

PAMAM dendrimers were synthesized according to the literature [14]. Ethylenediamine (10.0 g, 0.166 mol) was dissolved in 100 mL methanol. Methyl acrylate (0.751 mol (94.6 g) was added to above solution at 40 °C and the system stirred for 24 h under nitrogen. Excess methyl acrylate was removed under vacuum at room temperature. A Michael addition between the amine and the acrylate yielded a product bearing four terminal methyl ester groups. Subsequently, ethylenedi-

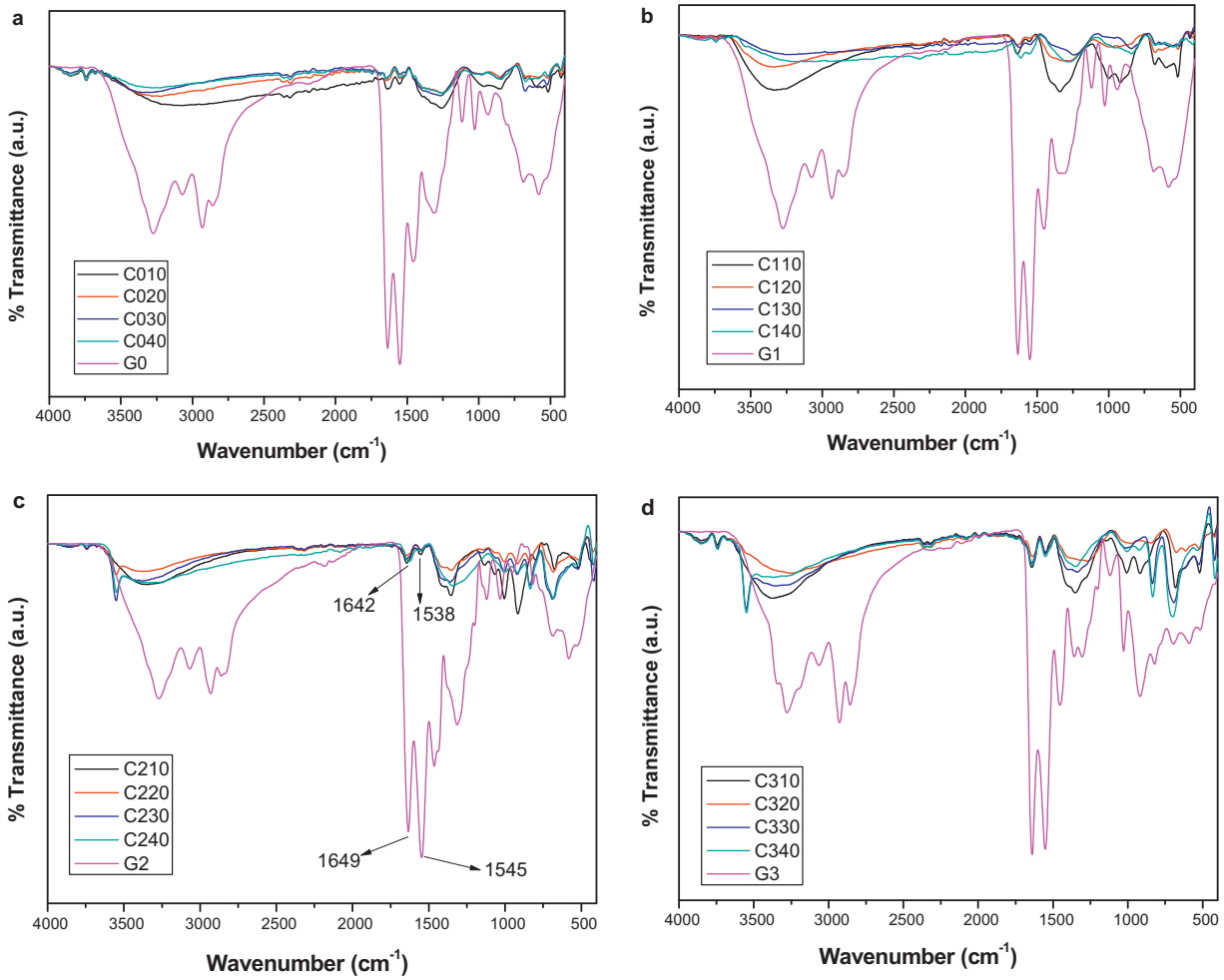

Fig. 4. FT-IR spectra of (a) Co–G0.0, (b) Co–G1.0, (c) Co–G2.0, (d) Co–G3.0 (the feed molar ratio of Co^{2+} to dendrimers is 10:1, 20:1, 30:1 and 40:1).

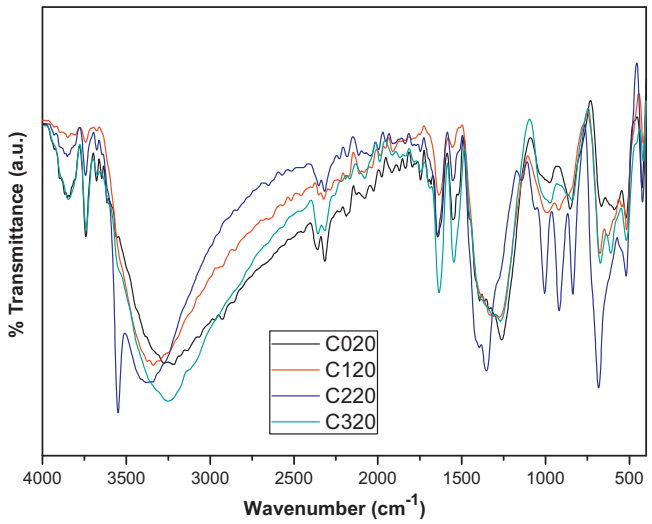

Fig. 5. FT-IR spectra of Co–G0–G3 (the feed molar ratio of Co^{2+} to dendrimers is 20:1).

Table 1
Some chemical and physical characteristic of dendrimers.

Generation	Molecular formula	Molecular weight ($g\,mol^{-1}$)	Number of terminal amino groups	Number of total amino groups
G0	$C_{22}H_{48}O_4N_{10}$	516	4	10
G1	$C_{62}H_{128}O_{12}N_{26}$	1429	8	26
G2	$C_{142}H_{288}O_{28}N_{58}$	3254	16	58
G3	$C_{302}H_{609}O_{60}N_{132}$	6905	32	122

Table 2
Denotation of dendrimer-encapsulated monometallic Co-nanoparticles.

Generation	Metal/Dendrimer molar ratio			
	10:1	20:1	30:1	40:1
G0	C010	C020	C030	C040
G1	C110	C120	C130	C140
G2	C210	C220	C230	C240
G3	C310	C320	C330	C340

amine (120 g, 2.00 mol) was dissolved in methanol and added to the four terminal methyl ester containing dendrimer, stirred for 48 h under nitrogen and excess reactants were removed by vacuum distillation. Then, product bearing four terminal amino groups were obtained, defined as the G0 PAMAM. By repeating the above cycle, higher generation PAMAM dendrimers (up to G3) were synthesized. Purity of the amine-terminated PAMAM dendrimers was characterized via FT-IR, 1H and ^{13}C NMR. The results agreed well with that reported in the literature [19]. The structures of dendrimers are given in Fig. 1. The characteristics and abbreviations are presented in Table 1.

2.3.2. The synthesis of Co nanoparticles via the template of dendrimers

Briefly, certain amount of $CoCl_2{\cdot}6H_2O$ dissolved in 10 mL of in Milli-Q water was added drop-wise into a 10 mL of 1 mM dendrimer (G0.0, 1.0, 2.0 and 3.0) solution, followed by further stirring for 2 h in order to drive the coordination reaction to completion (Fig. 2). The feed molar ratio of Co^{2+} to dendrimers is 10:1, 20:1, 30:1 and 40:1, respectively (Table 2). Afterwards, 10 mL of 0.3 M $NaBH_4$ solution (freshly prepared) was introduced into the above solution quickly, and then the mixture was stirred vigorously for 1 h. The solid was filtered, rinsed three times with Milli-Q water, and then dried under vacuum at 50 °C (Fig. 3).

As presented in Fig. 3, the Co NP's were prepared via a two-step sequence. The coordination of Co^{2+} ions with dendrimers and subsequent chemical reduction to produce Co NP's. After the coordination of Co^{2+} to the dendrimer, solution turns into green (Fig. 3a). When Co^{2+} ions were reduced into Co NP's, solution color becomes dark gray (Fig. 3b). This is an important indication of reduction of Co^{2+} ions into Co [20,21]. After the dispersion of solid product in an aqueous solution, they could be easily collected by magnet (Fig. 3c).

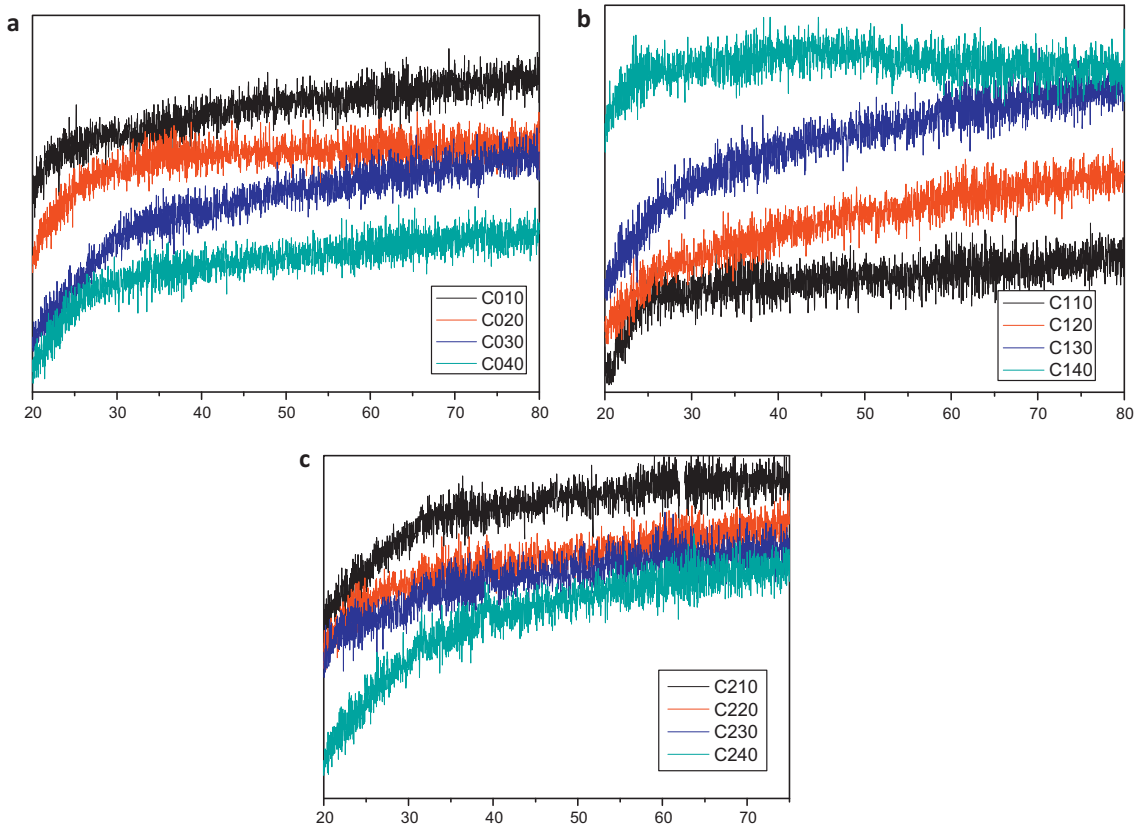

Fig. 6. XRD powder pattern of (a) Co–G0, (b) Co–G1, (c) Co–G2 (the feed molar ratio of Co^{2+} to dendrimers is 10:1, 20:1, 30:1 and 40:1).

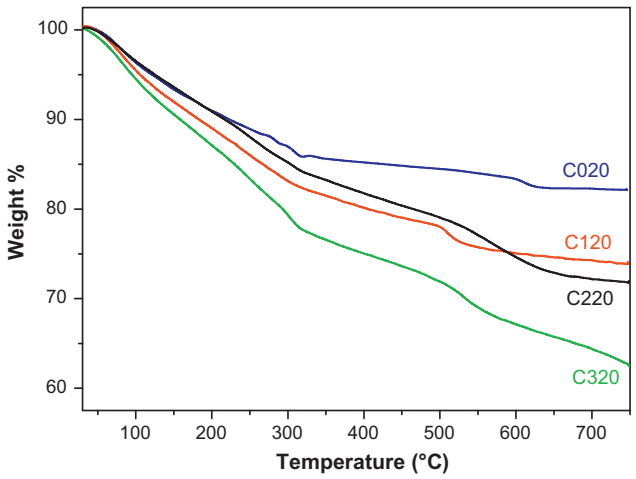

Fig. 7. TGA curves of Co–G0–G3 (the feed molar ratio of Co^{2+} to dendrimers is 20:1).

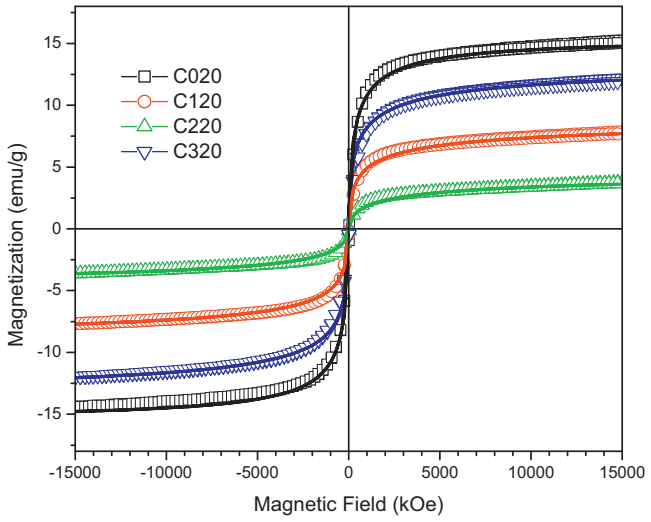

Fig. 9. M–H hysteresis curves of curves of Co–G0–G3 (the feed molar ratio of Co^{2+} to dendrimers is 20:1).

3. Results and discussion

3.1. FT-IR analysis

Fig. 4 shows the FT-IR spectra from the water solution of the dendrimers (G0–G3), the mixture of dendrimers and the cobalt ions; (a) G0–Co^{2+}, (b) G1–Co^{2+}, (c) G2–Co^{2+}, (d) G3–Co^{2+}. As it can be seen, the G0 to G3 dendrimers (Fig. 5) spectra exhibit two broad peaks centered at 1649 and 1545 cm^{-1}, assigned to the C=O stretching (amide I) and N–H bending/C–N stretching (amide II) vibrations of the dendrimers [22–25], respectively. The C–H stretch modes can be observed at 2945 cm^{-1} and 2842 cm^{-1}. When the cobalt ions are added into the solution of the dendrimers (G1–G3), the new bands corresponding to amide (–CO–NH–) I and II of G1–G3 dendrimers appear at 1642 cm^{-1} and 1538 cm^{-1}, respectively. These results strongly indicate that dendrimers still exist in the nanocomposite (coordination reaction between the cobalt ions and the nitrogen or oxygen atoms from amide groups when cobalt ions are introduced into the solution of the dendrimers) [24–26].

3.2. XRD analysis

The XRD powder patterns of Co–G1–G2 (the feed molar ratio of Co^{2+} to dendrimers is 10:1, 20:1, 30:1 and 40:1) were presented

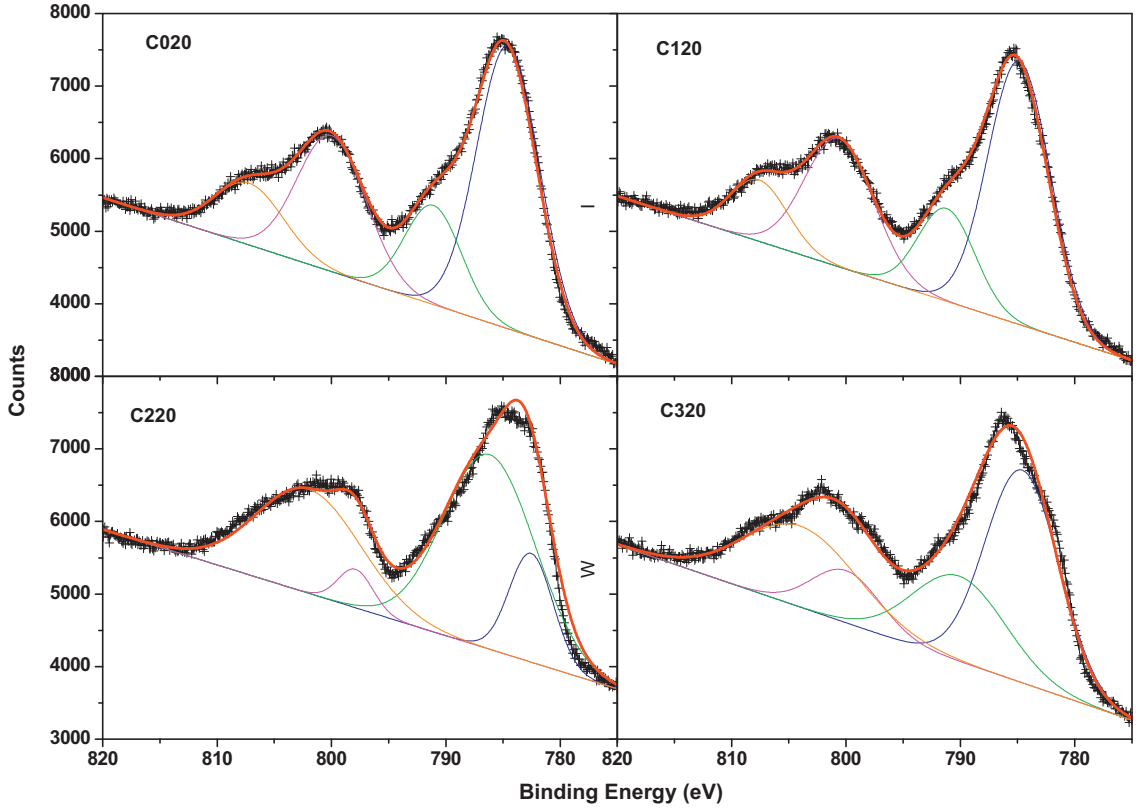

Fig. 8. XPS curves of Co–G0–G3 (the feed molar ratio of Co^{2+} to dendrimers is 20:1).

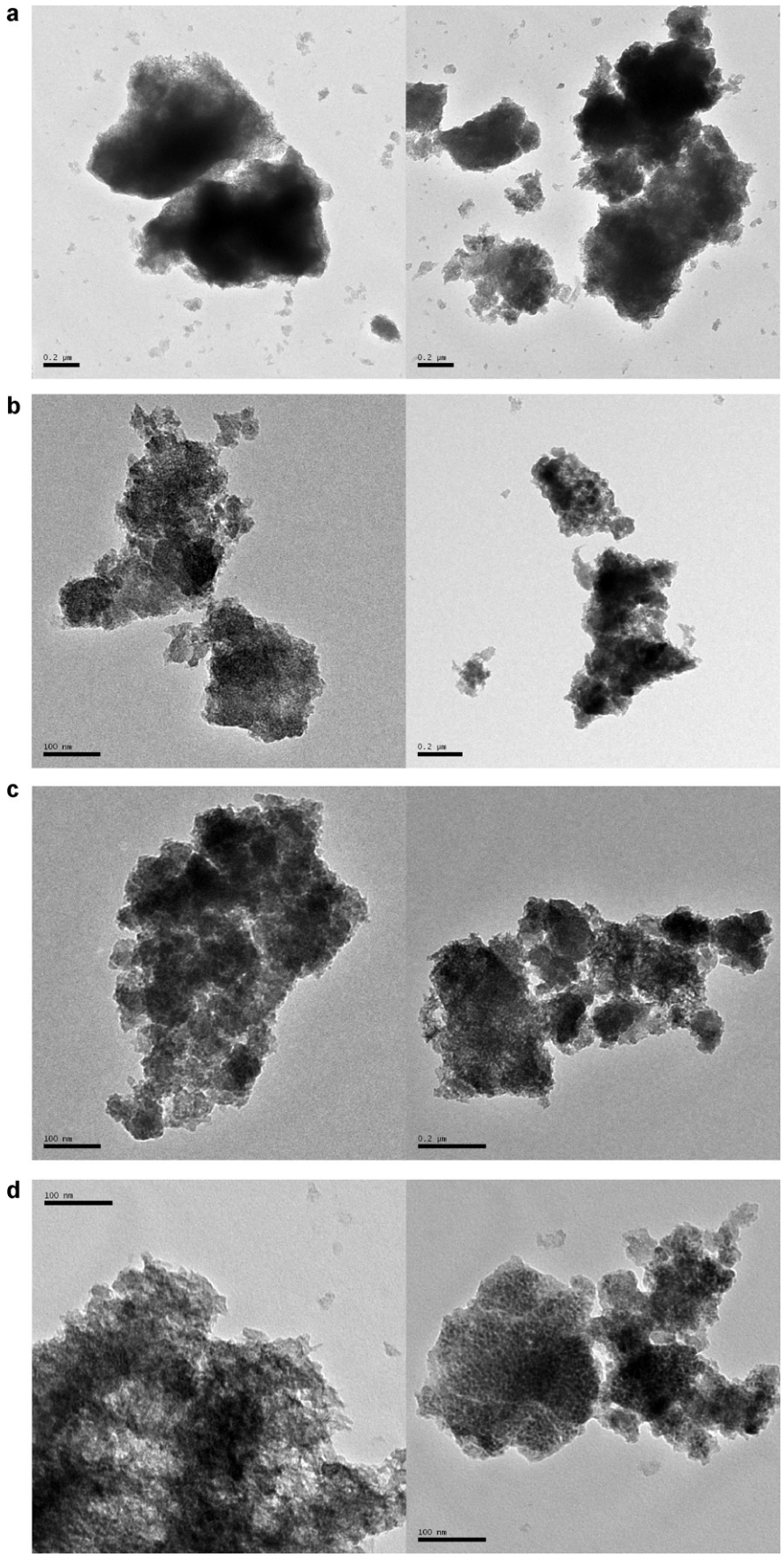

Fig. 10. TEM images of (a) Co–G0, (b) Co–G1, (c) Co–G2, (d) Co–G3 (the feed molar ratio of Co^{2+} to dendrimers is 20:1).

Table 3
Binding energies of Co $2p_{3/2}$ and Co $2p_{1/2}$ peaks for the samples.

Samples	Co $2p_{3/2}$ (eV)	Co $2p_{1/2}$ (eV)
C020	784.3	799.5
C120	784.6	800.1
C220	782.3	797.4
C320	784,2	799.5

in Fig. 6. All XRD patterns indicate that amorphous structure of all products. In any XRD powder patterns given in Fig. 6, there is no Bragg peak which indicate the crystalline structure of the products [21,27,28].

3.3. TG analysis

Thermal analysis was used to estimate the thermal stability of Co–G0–G3 (the feed molar ratio of Co^{2+} to dendrimers is 20:1) nanocomposite, and the obtained TGA curves (Fig. 7). About 14%, 16%, 19% and 22% weight gain in the temperature range of 100–400 °C can be observed in the TGA curve. The number of surface amines increased from dendrimer generations one to three. Gu et al. [29] stated that % weight loss is increasing, when dendrimer generation number is increased. And also similar behavior was also observed in Fig. 7.

3.4. XPS analysis

XPS measurements were carried out to gain more insight into the chemical covalent linkages on the surface of Co nanoparticles. The experimental XPS spectra of the samples have peaks with shoulder and the deconvoluted peaks were fitted by Gaussian functions (Fig. 8). The binding energies of Co $2p_{3/2}$ peaks are ascribed as 784.3, 784.6, 782.3 and 784,2 eV and that of Co $2p_{1/2}$ peaks are ascribed as 799.5, 800.1, 797.4 and 799.5 eV for C020, C120, C220 and C320, respectively (Table 3). The spin-orbital energies were calculated as 15.6, 15.7, 15.1 and 15.3 eV. The shake-up satellites are observed at higher energies of these peaks and found as 790.6, 790.7, 785.7 and 789.6 eV for $2p_{3/2}$, and 806.7, 807.1, 801.5 and 803.5 eV for $2p_{1/2}$.

In the literature the binding energies for Co 2p for different oxides, nitrides, chlorides, hydroxide and other complex of Co are reported as in Table 4. Also the shifting of binding energy toward the high energy values were observed with changing pH values of precursor solution [30–41]. All samples except C220 have close values of binding energies; it may be caused by different surface chemistry (hydroxide, oxide, boride or nitride of cobalt) of Co nano metals in C220 samples. The Co–O bonding vibration (in FTIR spectrum) peak is stronger in this sample when it is compared with that in others, so it can be inferred that Co has more oxidized surface in C220 than others. The binding energy value difference may be explained in the light of this fact.

Table 4
Binding energies (B.E.) for Co 2p of various oxides, nitrides, chlorides, hydroxides and other complexes of Co.

B.E. (eV)	Complex	Ref.
778.0	Co_2N	[31]
778.2	CoN	[31]
778.4	Co_2N_3	[31]
780.4	$Co(OH)_2$	[32]
781.2	CoO, $Co(OH)_2$, Co_2O_3	[33]
781.6	$Co(OH)_2$	[34]
781.9	$Co(OH)_2$	[33–36]
782.0	$Co(OH)_2$	[40]
782.1	Co(II) Chloride	[30]
782.6	Co_3O_4	[33]
783.2	$Co(OH)_2$	[33]
783.3	$Co(OH)_2$	[34–39]
783.6	Co_3O_4	[40]
783.6	$CoSiF_6$	[41]
787.6	$Co(OH)_2$	[40]
796.8	CoO, Co_2O_3	[33]
798.0	Co_3O_4, $Co(OH)_2$	[40]
798.2	$Co(OH)_2$	[33]
804.1	Co_2O_3	[40]

3.5. Magnetic measurements

The magnetization curves and their lognormal Langevien fits of all samples are shown in Fig. 9. The magnetization curves have superparamagnetic non hysteric characteristic at lower fields and with nonsaturation characteristic at high fields. The Co nanoparticles without dendrimer frame (C020) have saturation magnetization of 15.5 emu/g. The diamagnetic effect of surface spins to bulk spins, magnetically dead layers caused by oxidation of surface of Co may cause the decline of Ms with respect to the bulk Ms value of Co. The additional mass of dendrimers can be seen as a decrease of compound mass accordance with remaining mass of them at higher temperatures in TGA. By increasing the generation number dendrimer frame, the magnetization is generally decreasing except for C220. The obtained Ms values by extrapolation of Ms curves with 1/H are found as 13.7, 5 and 9.2 emu/g for C120, C220 and C320, respectively. Both XPS and FTIR analysis show that the different surface nature of Co for C220 sample. The surface including more oxides of Co cause the antiferromagnetic alignment of surface spins around the Co ferromagnetic core. The more oxidized surface may contribute the total magnetization with reducing effect for C220 sample.

3.6. TEM analysis

The successful formation of Co nanoparticles via the reduction of Co^{2+} under the template of dendrimers was first confirmed by TEM studies. Fig. 10 shows the TEM micrographs of Co nanoparticles obtained using different generation of dendrimers (G0.0–G3.0) as templates with the same feed molar ratio (20:1) of Co^{2+} to dendrimers. The Co particles aggregated easily, probably because of the high mobility of the particles as well as the magnetic interaction between the particles [42].

4. Conclusions

The cobalt nanoparticles are obtained and characterized using PAMAM dendrimers as templates. XRD analysis showed that the amorphous structure of the all products and FT-IR analysis proved the presence of between dendrimer and Co nanoparticles. The diamagnetic effect of surface spins to bulk spins, magnetically dead layers caused by oxidation of Co surface may cause the decline of Ms with respect to the bulk Ms value of Co.

Acknowledgements

The authors are thankful to the Fatih University, Research Project Foundation (Contract no: P50020902-2) and Turkish Ministry of Industry and TUBITAK (Contract no: 110T487) for financial support of this study, to Dr. Özgür DUYGULU for TEM measurements.

References

[1] J. Heidmann, A.M. Taratorin, Handbook of Magnetic Materials, vol. 19, 2011, 1.
[2] C.W. Thiel, T. Böttger, R.L. Cone, J. Lumin. (2011), doi:10.1016/j.jlumin.2010.12.015.
[3] B. Zhang, J. Cheng, X. Gong, X. Dong, X. Liu, G. Ma, J. Chang, J. Colloid Interface Sci. 322 (2008) 485.

[4] S. Othmani, R. Blel, M. Bejar, M. Sajieddine, E. Dhahri, E.K. Hlil, Solid State Commun. 149 (2009) 969.
[5] M.F. Casula, A. Corrias, P. Arosio, A. Lascialfari, T. Sen, P. Floris, I.J. Bruce, J. Colloid Interface Sci. (2011), doi:10.1016/j.jcis.2011.01.088.
[6] H. Ito, R. Kato, K. Ino, H. Honda, J. Biosci. Bioeng. 109 (2010) 182.
[7] B. Fenga, R.Y. Honga, Y.J. Wua, G.H. Liuc, L.H. Zhongb, Y. Zhengd, J.M. Dinge, D.G. Wei, J. Alloys Compd. 473 (2009) 356.
[8] S. Laurent, D. Forge, M. Port, A. Roch, C. Robic, L.V. Elst, R.N. Muller, Chem. Rev. 108 (2008) 2064.
[9] L. Jin, S. Yang, Q. Tian, H. Wu, Y. Cai, Mater. Chem. Phys. 112 (2008) 977.
[10] R.C. Hedden, B.J. Bauer, A.P. Smith, F. Grohn, E. Amis, Polymer 43 (2002) 5473.
[11] Y. Niu, H. Lu, D. Wang, Y. Yue, S. Feng, J. Organomet. Chem. 696 (2011) 544.
[12] O. Ozturk, T.J. Black, K. Perrine, K. Pizzolato, C.T. Williams, F.W. Parsons, J.S. Ratliff, J. Gao, C.J. Murphy, H. Xie, H.J. Ploehn, D.A. Chen, Langmuir 21 (2005) 3998.
[13] B. Natarajan, N. Jayaraman, J. Organomet. Chem. 696 (2011) 722.
[14] Y. Niu, R.M. Crooks, C. R. Chim. 6 (2003) 1049.
[15] Y.J. Jin, Y.J. Luo, G.P. Li, J. Li, Y.F. Wang, R.Q. Yang, W.T. Lu, Forensic Sci. Int. 179 (2008) 34.
[16] L. Balogh, R. Valluzzi, G.L. Hagnauer, K.S. Laverdure, S.P. Gido, D.A. Tomalia, J. Nanopart. Res. 1 (1999) 353.
[17] M.F. Ottaviani, R. Valluzzi, L. Balogh, Macromolecules 35 (2002) 5105.
[18] Y.Y. Cheng, D.Z. Chen, R.Q. Fu, Polym. Int. 54 (2005) 495.
[19] D.A. Tomalia, A.M. Naylor, W.A. Goddard, Angew. Chem. 29 (1990) 138.
[20] Y. Chen, K.Y. Liev, J.L. Li, Appl. Surf. Sci. 255 (2009) 4039.
[21] H.X. Wu, C.X. Zhang, L. Jin, H. Yang, S.P. Yang, Mater. Chem. Phys. 121 (2010) 342.
[22] H.M. Tan, Y.J. Luo, Dendritic Polymer, Chemical Industry Press, Beijing, 2002.
[23] G. Socrates, Infrared and Raman Characteristic Group Frequencies: Tables and Charts, 3rd ed., Wiley, Chichester, 2001.
[24] L. Jin, S. Yang, Q.W. Tiana, H.X. Wua, Y.J. Cai, Mat. Chem. Phys. 112 (2008) 977.
[25] T. Endo, T. Yoshimura, K. Esumi, J. Colloid Interface Sci. 286 (2005) 602.
[26] D.X. Liu, J.X. Gao, J.C. Murphy, T.C. Williams, J. Phys. Chem. B 108 (2004) 12911.
[27] K. Yasui, T. Morikawa, K. Nishio, H. Masuda, Jpn. J. Appl. Phys. 44 (2005) L469.
[28] J.X. Xu, Y. Xu, Mater. Lett. 60 (2006) 2069.
[29] B.F. Pan, F. Gao, H.C. Gu, J. Colloid Interface Sci. 284 (2005) 1.
[30] J.G. Dillard, M.H. Koppelman, J. Colloid Interface Sci. 87 (1982) 56.
[31] W. De La Cruz, O. Contreras, G. Soto, E.P. Tijerina, Revista Mexicana De Fisica 52 (5) (2006) 409.
[32] Y.P. Wang, Y.J. Wang, Q.L. Ren, L. Li, L.F. Jiao, D.W. Song, G. Liu, Y. Han, H.T. Yuan, Fuel Cells 10 (2010) 510.
[33] C.H. Liu, B.H. Chen, C.L. Hsueh, J.R. Ku, F. Tsau, K.J. Hwang, Appl. Catal. B 91 (2009) 368.
[34] N. Patel, G. Guella, A. Kale, A. Miotello, B. Patton, C. Zanchetta, L. Mirenghi, P. Rotolo, Appl. Catal. A 323 (2007) 18.
[35] N. Patel, R. Fernandes, G. Guella, A. Kale, A. Miotello, B. Patton, C. Zanchetta, J. Phys. Chem. 112 (2008) 6968.
[36] N. Patel, R. Fernandes, A. Miotello, J. Power Sources 188 (2009) 411.
[37] R. Fernandes, N. Patel, A. Miotello, M. Filippi, J. Mol. Catal. A: Chem. 298 (2009) 1.
[38] R. Fernandes, N. Patel, A. Miotello, Appl. Catal. B 92 (2009) 68.
[39] R. Fernandes, N. Patel, A. Miotello, Int. J. Hydrogen Energy 34 (2009) 2893.
[40] C.H. Liu, Y.C. Kuo, B.H. Chen, C.L. Hsueh, K.J. Hwang, J.R. Ku, F. Tsau, M.S. Jeng, Int. J. Hydrogen Energy 35 (2010) 4027.
[41] T. Sekine, N. Ikeo, Y. Nagasawa, Appl. Surf. Sci. 100/101 (1996) 30.
[42] Y. Chen, K.Y. Liew, J.L. Li, Appl. Surf. Sci. 255 (2009) 4039.